JOURNAL OF Materials CHEMISTRY

Surface-limited ionic transport in perovskites $Sr_{0.97}(Ti,Fe,Mg)O_{3-\delta}$

V. V. Kharton,*[a,b] A. P. Viskup,[a] A. V. Kovalevsky,[a] F. M. Figueiredo,[b] J. R. Jurado,[c] A. A. Yaremchenko,[a] E. N. Naumovich[a] and J. R. Frade[b]

[a]*Institute of Physicochemical Problems, Belarus State University, 14 Leningradskaya Str., 220080 Minsk, Republic of Belarus. E-mail: kharton@cv.ua.pt or kharton@fhp.bsu.unibel.by*
[b]*Department of Ceramics and Glass Engineering, UIMC, University of Aveiro, 3810 Aveiro, Portugal*
[c]*Instituto de Ceramica y Vidrio, CSIC, Arganda del Rey, Madrid, Spain*

Received 9th December 2000, Accepted 8th February 2000
Published on the Web 4th April 2000

Oxygen permeation and faradaic efficiency measurements of perovskite solid solutions $Sr_{0.97}Ti_{1-x-y}Fe_xMg_yO_{3-\delta}$ ($x=0.20$–0.40; $y=0$–0.10) at 973–1223 K showed that the oxygen transport at membrane thicknesses below 2 mm is limited by both bulk ionic conductivity and the surface exchange kinetics. Incorporation of either iron or magnesium into the B sublattice of strontium titanate results in greater p-type electronic and oxygen ionic conductivities. For $Sr_{0.97}(Ti,Fe)O_{3-\delta}$ solid solutions, the role of the surface exchange as the permeation-determining factor decreases with reducing temperature. In contrast, the limiting effect of the interphase exchange on oxygen transport through $Sr_{0.97}Ti_{0.70}Fe_{0.20}Mg_{0.10}O_{3-\delta}$ membranes is observed to be significant within the studied temperature range, suggesting that doping with magnesium leads to higher ionic conductivity and lower surface exchange rates in comparison with $Sr_{0.97}Ti_{0.60}Fe_{0.40}O_{3-\delta}$ perovskite which exhibit similar permeation fluxes. The ion transference numbers of the solid solutions in air, estimated from the oxygen permeation and faradaic efficiency results, do not exceed 0.14. TGA/DTA results demonstrated the stability of the perovskite phases in CO_2-containing atmospheres at temperatures above 770 K. The effect of the surface exchange limitations on the faradaic efficiency results is analysed.

Introduction

Mixed ionic–electronic conductors with the ABO_3 perovskite structure, derived from alkaline-earth titanates $ATiO_{3-\delta}$ (A = Sr, Ca, Ba), are of considerable interest as materials for high-temperature electrochemical cells such as dense ceramic membranes for oxygen separation and partial oxidation of hydrocarbons, electrodes for solid oxide fuel cells (SOFCs), and sensors.[1–16] The promising features of the titanate-based ceramics include their stability under a wide range of oxygen chemical potentials, and a significant oxygen-ion mobility coupled with dominant p-type electronic conductivity at high oxygen partial pressures and n-type conductivity under reducing environments. In addition, the large number of titanate-based applications has resulted in well-developed processing technologies and a detailed understanding of the physicochemical properties of these materials, thus reducing costs for their use in the high-temperature electrochemical devices.

Substituting titanium in the B sublattice with lower-valency transition metal cations, such as iron or cobalt, leads to higher oxygen ionic and electron–hole conduction. The increase in ionic conductivity is due to both higher oxygen deficiency and weaker B–O bonds.[1,6,7,9,13] As a result, the oxygen permeation fluxes through $Sr(Ti,B)O_{3-\delta}$ (B = Fe, Co) ceramic membranes increase regularly with increasing concentration of cobalt or iron.[6,9] Oxygen transport through strontium titanate-based ceramics was found to be limited by both bulk ionic conduction and surface exchange rates at the oxide/gas phase boundaries.[6,15]

Among the main disadvantages of the alkaline-earth element containing perovskites as materials of electrochemical cells is their reactivity with gas species such as carbon dioxide,[3,9,16,17] which is present in atmospheric air and in products of hydrocarbon oxidation. The creation of a moderate cation deficiency in the A sublattice may be considered as a possible method to improve the stability of such materials with respect to the interaction with CO_2 .[3,9,17]

In our previous works,[9,18] the ionic transport properties of $SrTi_{1-x}Fe_xO_{3-\delta}$ perovskites were studied by oxygen permeation and faradaic efficiency measurements. The stability in CO_2-containing atmospheres and thermal expansion were also addressed as key factors for their potential use in high-temperature electrochemical applications.[18] We now extend this study to heavily iron-doped and magnesium-doped compositions in the system $Sr_{0.97}Ti_{1-x-y}Fe_xMg_yO_{3-\delta}$. Since the ionic conductivity of $Sr(Ti,Fe)O_{3-\delta}$ phases increases with increasing oxygen nonstoichiometry,[9] the incorporation of bivalent magnesium cations into the titanium sublattice was considered as a possible strategy for enhancing the oxygen vacancy concentration and, thus, oxygen permeation fluxes. Also, the relationships between the results on oxygen permeation and faradaic efficiency for the case when surface exchange limitations are considerable, are discussed using the $Sr(Ti,Fe,Mg)O_{3-\delta}$ solid solutions as a model.

Experimental

1 Synthesis and characterization

Solid-state synthesis of $Sr_{0.97}Ti_{1-x-y}Fe_xMg_yO_{3-\delta}$ ($x=0.20$–0.40; $y=0$–0.10) was performed by a standard ceramic technique using high-purity $SrCO_3$, TiO_2 and $FeC_2O_4{\cdot}2H_2O$ or Fe_3O_4 as starting materials. The prepared compositions and corresponding abbreviations are listed in Table 1. After thermal pre-treatment of the stoichiometric mixtures, the oxides were pressed into bars ($4\times4\times30$ mm^3) and disks of different thickness (10 to 20 mm in diameter) and then sintered in air at 1520–1720 K for 4–20 hours. The density of the ceramic samples (ρ_{exp}) was no less than 95% of the theoretical density (ρ_{theor}) estimated from the X-ray diffraction (XRD) data (Table 1). The prepared samples were characterized using

Table 1 Abbreviations and properties of $Sr_{0.97}Ti_{1-x-y}Fe_xMg_yO_{3-\delta}$ ceramics

Composition				
x	y	Abbreviation	Unit cell parameter, a/nm (± 0.0001 nm)	ρ_{exp}/ρ_{theor} (%)
0.20	0	STF20	0.3905	98.5
0.20	0.10	STF2M1	0.3907	95.5
0.40	0	STF40	0.3898	96.5

XRD, X-ray fluorescence analysis (XFA), emission spectroscopic analysis, differential thermal analysis (DTA), thermal gravimetric analysis (TGA), and infrared (IR) absorption spectroscopy. The experimental procedures used for this characterization as well as testing gas tightness, measuring electrical conductivity and thermal expansion are described in detail elsewhere.[6,8,19–23] Only gas-tight ceramic samples were used for the oxygen permeation and faradaic efficiency measurements.

2 Oxygen permeation measurements

Steady-state oxygen permeation (OP) fluxes were measured using an experimental technique based on stabilized zirconia electrochemical cells consisting of an oxygen pump and sensor, as described in detail earlier.[6,8,9,19,21,22] The permeation was studied at 973–1223 K in the range of oxygen partial pressures at the membrane permeate side (p_1) from 0.1 Pa to 1.5×10^4 Pa. The feed-side reference oxygen pressure (p_2) was 2.1×10^4 Pa (atmospheric air). The thickness of the membrane samples (d) was varied from 0.6 to 2.0 mm.

The discussion of permeation results will be based on the quantities of oxygen permeation flux density (mol s^{-1} cm^{-2}) and specific oxygen permeability (mol s^{-1} cm^{-1}) defined as[24]

$$J(O_2)=j\cdot d\cdot\left[\ln\frac{p_2}{p_1}\right]^{-1} \quad (1)$$

The oxygen partial pressure at the membrane permeate side was calculated from the e.m.f. (E) of the oxygen sensor according to the Nernst law:

$$E=\frac{RT}{4F}\cdot\ln\left(\frac{p_2}{p_1}\right) \quad (2)$$

The quantity $J(O_2)$ is convenient in order to identify the limiting effect of the oxygen surface exchange rate on the oxygen permeation, on the basis of the thickness dependence of the permeation flux.[8,25] Since the oxygen permeability is proportional to $j\times d$, $J(O_2)$ is expected to be thickness-independent when the kinetics of surface exchange processes is fast. In this case, the physical meaning of the oxygen permeability quantity should refer to the ambipolar conductivity (σ_{amb}) of the membrane material, averaged for a given oxygen partial pressure range:

$$J(O_2)=\frac{RT}{16F^2}\cdot\overline{\sigma_{amb}}=\frac{RT}{16F^2}\cdot\frac{\overline{\sigma_o\cdot\sigma_e}}{\sigma_o+\sigma_e}=\frac{RT}{16F^2}\cdot\overline{\sigma\cdot t_o(1-t_o)} \quad (3)$$

where t_o is the oxygen ion transference number, and σ, σ_o and σ_e are the total, oxygen ionic and electronic conductivities, respectively. If permeation is limited by slow surface exchange, $J(O_2)$ should increase with increasing membrane thickness for a given oxygen chemical potential gradient. As both ionic conductivity and exchange currents are functions of oxygen chemical potential,[6–8,19–22] the values of $J(O_2)$ are presented hereafter in combination with the corresponding values of p_1 and p_2.

For some membrane samples, steady state was attained after long periods of time (150 to 200 h), an observation probably caused by processes of local ordering in the oxygen sublattice. After starting the oxygen permeation experiments, the oxygen flux through such membranes slowly decreased with time, as illustrated by Fig. 1. Taking this transient regime into account, we used the time independence of the sensor e.m.f. during 20–40 h (with a drift less than 1% under constant current through the oxygen pump) as a criterion for steady-state attainment.

3 Faradaic efficiency measurements

The experimental technique used in this work for faradaic efficiency (FE) studies has been described elsewhere.[26] The YSZ electrochemical cells for faradaic efficiency tests were similar to the cell for the oxygen permeability studies, consisting of an oxygen pump, a sensor and a dense membrane sample with porous Pt electrodes sealed onto the cell. The feed-side oxygen partial pressure during faradaic efficiency measurements was 2.1×10^4 Pa.

In the course of the measurements, the oxygen permeation flux through the membrane was first determined at the required temperature and permeate-side oxygen pressure. For this purpose, a direct current (I_{out}) was passed through the pump, removing oxygen from the cell, while the circuit with the sample under study was open. After the sensor e.m.f. (E) became time-independent, the permeation flux (J/mol s^{-1}) for the given conditions (T and p_1) was proportional to the current through the oxygen pump:

$$J=I_{out}\cdot(4F)^{-1} \quad (4)$$

Then a direct current (I_{in}) was passed through the membrane sample to pump oxygen into the cell, and I_{out} was adjusted to provide the same value of E, independent of time. In this case the sum of the oxygen fluxes, driven through the membrane by the electrical and chemical potential differences (J_{in} and J, respectively), is equal to the flux through the pump:

$$I_{out}\cdot(4F)^{-1}=J_{in}+J=t_o\cdot I_{in}\cdot(4F)^{-1}+J \quad (5)$$

Oxygen ion transference numbers at the given E value can be, therefore, determined as

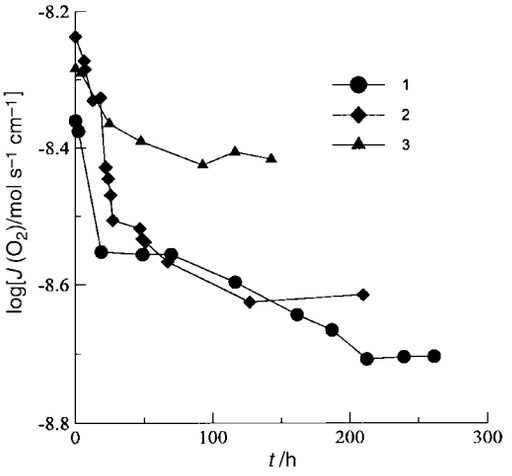

Fig. 1 Time dependence of oxygen permeability after placing membranes under an oxygen pressure gradient ($p_2=0.21$ atm): (1), STF2M1, $d=0.60$ mm, 1173 K; (2), STF40, $d=1.28$ mm, 1223 K; (3), STF40, $d=1.00$ mm, 1223 K. The permeate-side oxygen pressure was $(1.9\pm0.2)\times10^{-2}$ atm.

$$t_o = \frac{I_{out} - 4FJ}{I_{in}} \quad (6)$$

To determine the oxygen ion transference numbers in air, I_{out} was adjusted to provide the condition

$$E \approx 0 \quad (7)$$

at a given value of I_{out}. In this case the oxygen fluxes through the membrane and the pump are equivalent

$$I_{out} \cdot (4F)^{-1} = J_{in} = t_o \cdot I_{in} \cdot (4F)^{-1} \quad (8)$$

and

$$t_o = I_{out}/I_{in} \quad (9)$$

The faradaic efficiency measurements were performed in the same temperature range as was used for oxygen permeability measurements. The time necessary for steady-state attainment was similar to that for the steady permeation flux measurements.

As mentioned for the oxygen permeability measurements, slow surface exchange may also influence the results of faradaic efficiency studies; this effect is analysed below.

Results and discussion

1 Materials characterization

XRD analysis of $Sr_{0.97}Ti_{1-x-y}Fe_xMg_yO_{3-\delta}$ showed that all materials were single phase with a typical cubic perovskite structure. The calculated unit cell parameters (a) are listed in Table 1. Substitution of titanium with iron leads to a smaller unit cell volume, while incorporation of magnesium cations into the B sublattice results in a slight increase in the lattice parameter. Such behavior is in agreement with the changes of average ionic radii of the B-site cations. No considerable changes in the lattice parameter or in the phase composition were found after keeping the samples under ambient conditions for 20–30 days.

The Arrhenius plots of total conductivity of $Sr_{0.97}Ti_{1-x-y}Fe_xMg_yO_{3-\delta}$ ceramics in air (Fig. 2) show that the conductivity increases when titanium is substituted with either iron or magnesium. At temperatures above 1000–1100 K, all the ceramics exhibit a transition to metallic-type conductivity, in good agreement with preliminary results.[3] The activation energy for the electrical conductivity (E_a) was calculated using the standard Arrhenius model:

$$\sigma = \frac{A_0}{T} \cdot \exp\left(-\frac{E_a}{RT}\right) \quad (10)$$

where A_0 is the pre-exponential factor. The solid lines in Fig. 2 result from the fit to eqn. (10); the fitting parameters are listed in Table 2. In the low-temperature range ($T < 1000$ K), the activation energy is close to 50 kJ mol^{-1} for $Sr_{0.97}Ti_{0.80}Fe_{0.20}O_{3-\delta}$ and $Sr_{0.97}Ti_{0.70}Fe_{0.20}Mg_{0.10}O_{3-\delta}$, being as low as 35 kJ mol^{-1} for $Sr_{0.97}Ti_{0.60}Fe_{0.40}O_{3-\delta}$. Note that the adequacy of the Arrhenius model for describing the conductivity of STF40 as a function of temperature is poorer with respect to STF20 and STF2M1 (Fig. 2 and Table 2), suggesting a more complex conduction mechanism. One can assume that the electronic conduction in $Sr_{0.97}Ti_{0.80}Fe_{0.20}O_{3-\delta}$ and $Sr_{0.97}Ti_{0.70}Fe_{0.20}Mg_{0.10}O_{3-\delta}$ in the low-temperature range occurs predominantly *via* transport of p-type small polarons between iron ions; doping $Sr_{0.97}(Ti,Fe)O_{3-\delta}$ with magnesium increases the Fe^{4+} concentration and, thus, leads to increasing concentration of mobile electronic charge carriers. In contrast, increasing the iron content in the perovskite lattice results in delocalization of the atomic levels of B cations and increases the bandwidth; this is confirmed by the decreasing activation energy for electronic conduction (Table 2) and reducing the temperature of the transition to metallic behavior (Fig. 2).

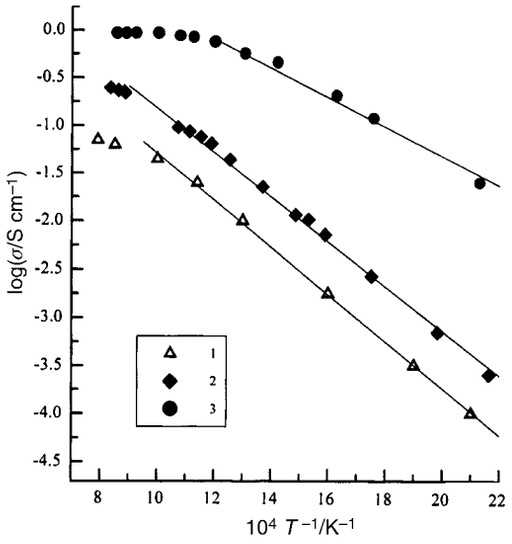

Fig. 2 Temperature dependence of the total electrical conductivity in air: (1), $Sr_{0.97}Ti_{0.80}Fe_{0.20}O_{3-\delta}$, (2), $Sr_{0.97}Ti_{0.70}Fe_{0.20}Mg_{0.10}O_{3-\delta}$, (3), $Sr_{0.97}Ti_{0.60}Fe_{0.40}O_{3-\delta}$.

2 Stability in CO_2 atmospheres

Preliminary tests demonstrated the stability of $Sr_{0.97}Ti_{1-x-y}Fe_xMg_yO_{3-\delta}$ phases in CO_2-containing atmospheres at temperatures above 770 K. For example, Fig. 3 presents the TGA results for $Sr_{0.97}Ti_{0.60}Fe_{0.40}O_{3-\delta}$ powders, obtained by crushing single-phase ceramics, in different gas mixtures. For comparison, the results of similar tests on SrO are given in Fig. 3D. Before the testing, all the samples were annealed in air at 1070–1250 K in the TGA cell. After such pretreatment, they were slowly cooled to the temperature of the experiment and tested for 10–12 hours in CO_2-containing atmospheres. Within the experimental error limits, no interaction between STF40 and carbon dioxide was found by TGA at 770–1070 K, whereas the reaction of strontium carbonate formation from SrO occurs extensively. DTA results for the STF40 powders, kept in a CO_2 atmosphere for various times, also showed no thermal effects in the heating mode. This suggests that adsorption of CO_2 on the surface of the solid solutions does not result in considerable decomposition of the perovskite phase.

On the other hand, IR absorption studies of the $Sr_{0.97}Ti_{1-x-y}Fe_xMg_yO_{3-\delta}$ powders indicated the presence of traces of $SrCO_3$ after the powder had been kept in the carbon dioxide atmosphere at room temperature. As an example, Fig. 4 shows the IR spectra of single-phase $Sr_{0.97}Ti_{0.70}Fe_{0.20}Mg_{0.10}O_{3-\delta}$ powder before and after storage in a CO_2 atmosphere. The spectrum of the reacted sample exhibits IR absorption bands at $\nu \sim 890$ and $\nu \sim 1080$ cm^{-1}, which can be related to the presence of strontium carbonate.[27] The intensity of the second peak increases with increasing time of exposure to CO_2. Similar behavior was observed in the case of $Sr_{0.97}Ti_{0.60}Fe_{0.40}O_{3-\delta}$ powders. Therefore, surface decomposition of the perovskite phase due to interaction with carbon dioxide may

Table 2 Parameters of the regression model eqn. (10) for the temperature dependence of the electrical conductivity of $Sr_{0.97}Ti_{1-x-y}Fe_xMg_yO_{3-\delta}$ ceramics in air

x	y	T/K	E_a/kJ mol^{-1}	ln(A_0)/S cm^{-1}
0.20	0	400–1170	49.4 ± 0.7	9.6 ± 0.1
0.20	0.10	450–1100	51 ± 1	11.1 ± 0.2
0.40	0	470–890	35 ± 3	11.5 ± 0.6

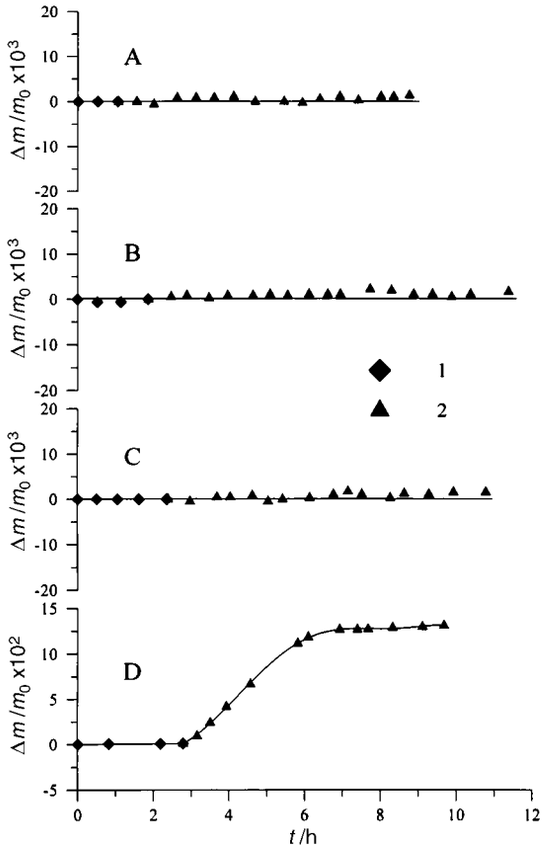

Fig. 3 Relative weight changes of $Sr_{0.97}Ti_{0.60}Fe_{0.40}O_{3-\delta}$ (A, B and C) and SrO (D) in different atmospheres at 1073 K (A), 885 K (B), 780 K (C), and 823 K (D): (1), atmospheric air purified from CO_2, (2), mixture of CO_2, O_2 and N_2. The ratio between O_2, CO_2 and N_2 concentrations was 14 : 18 : 68 (A and B), 19 : 17 : 64 (C and D).

still take place at low temperatures. However, sintered ceramic samples did not show any evidence of degradation after several months.

3 Oxygen permeability

The results on oxygen permeation through dense $Sr_{0.97}Ti_{1-x-y}Fe_xMg_yO_{3-\delta}$ ceramics as a function of temperature, permeate-side oxygen pressure and thickness are presented in Figs. 5–9. The general trends observed in these figures suggest that doping with either iron or magnesium lead to an increase of the permeation flux. This may be caused by the increase in vacancy concentration in the oxygen sublattice due to the reduction of the average oxidation state of B-site cations, which results in increasing oxygen ionic conductivity. In the temperature range from 973 to 1223 K, the oxygen permeability of $Sr_{0.97}Ti_{0.70}Fe_{0.20}Mg_{0.10}O_{3-\delta}$ ceramics was similar to that of $Sr_{0.97}Ti_{0.60}Fe_{0.40}O_{3-\delta}$. This fact might indicate close-related values of oxygen nonstoichiometry in the two compositions. At the same time, the dependence of the oxygen flux on the membrane thickness (Fig. 5) is a clear indication of the importance of surface exchange processes. As the ionic transport numbers are relatively low (Table 3), the bulk oxygen transport should be determined by the ionic conductivity. Thus, the permeation fluxes through $Sr_{0.97}(Ti,Fe,Mg)O_{3-\delta}$ should be limited by both surface exchange and oxygen ionic conductivity.

Additional measurements were carried out using surface-modified membranes which had been submitted to applying porous layers of either the same composition or a mixture of dispersed platinum and praseodymium oxide onto the feed-side surface (Figs. 6, 7 and 9). Details on the techniques of surface modification were reported elsewhere.[15,18] In fact, the surface

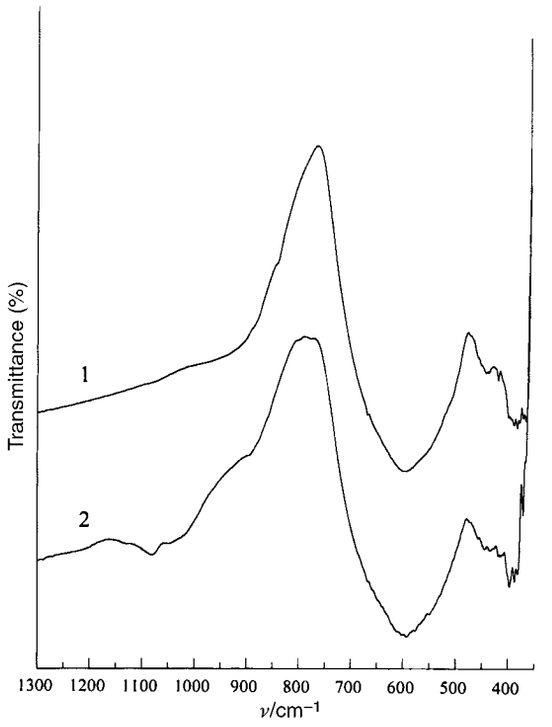

Fig. 4 IR absorption spectra of $Sr_{0.97}Ti_{0.70}Fe_{0.20}Mg_{0.10}O_{3-\delta}$ at room temperature: (1) after annealing in air at 1170 K for 2 h, (2) after keeping in CO_2 atmosphere at room temperature for 24 h. The spectra were obtained using samples of the same powder before and after its treatment in CO_2.

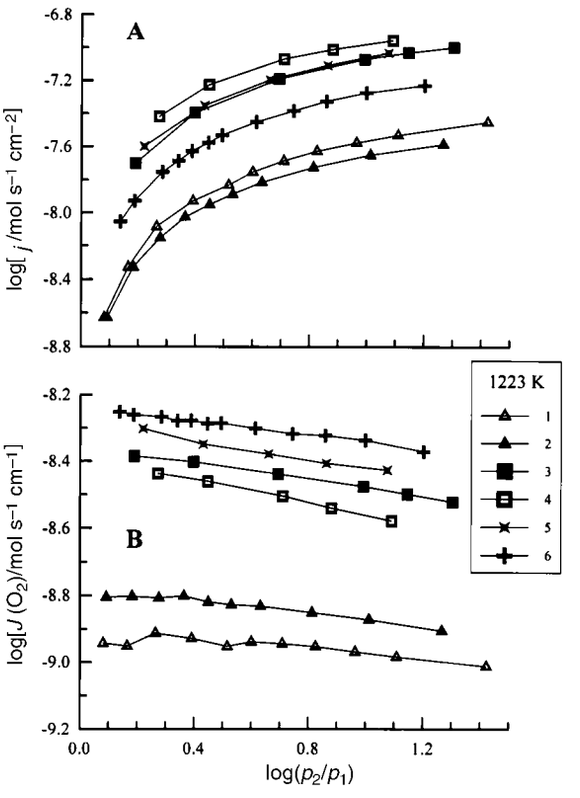

Fig. 5 Dependence of the oxygen permeation flux density (A) and specific oxygen permeability (B) on the oxygen partial pressure gradient at 1223 K and $p_2 = 0.21$ atm: (1), STF20, $d = 0.90$ mm; (2), STF20, $d = 1.40$ mm; (3), STF2M1, $d = 0.90$ mm; (4), STF2M1, $d = 0.60$ mm; (5), STF40, $d = 1.00$ mm; (6), STF20, $d = 2.00$ mm. Curve 2 corresponds to the membrane with the porous STF20 layer applied onto the feed-side surface.

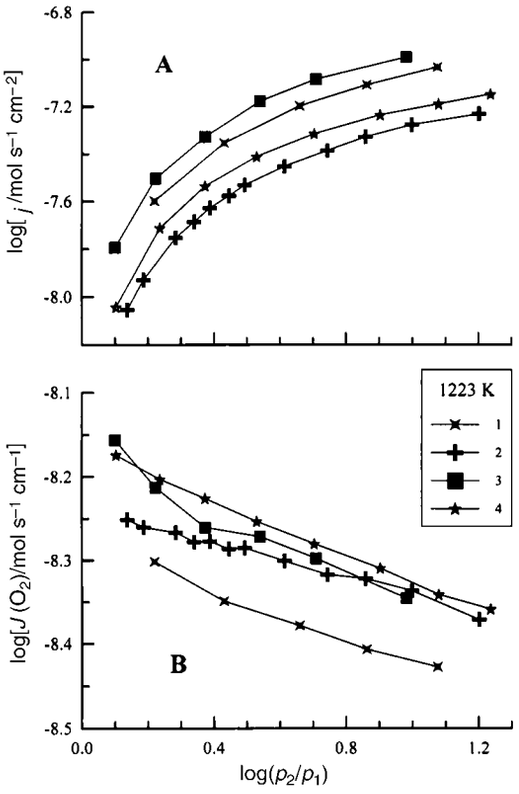

Fig. 6 Dependence of the oxygen permeation flux density (A) and specific oxygen permeability (B) of the $Sr_{0.97}Ti_{0.60}Fe_{0.40}O_{3-\delta}$ membranes on the oxygen pressure gradient at 1223 K and $p_2 = 0.21$ atm: (1), $d = 1.00$ mm; (2), $d = 2.00$ mm; (3), $d = 1.00$ mm, membrane with the Pt/PrO_x layer applied onto the feed-side surface; (4), $d = 1.75$ mm, membrane with the porous $Sr_{0.97}Ti_{0.60}Fe_{0.40}O_{3-\delta}$ layer applied onto the feed-side surface.

modification of the $Sr_{0.97}Ti_{1-x-y}Fe_xMg_yO_{3-\delta}$ membranes leads to a considerable increase of the oxygen permeability, especially at 1223 K (Fig. 6), thus confirming the permeation-determining role of the oxygen surface exchange.

One should note that $Sr_{0.97}Ti_{1-x}Fe_xO_{3-\delta}$ ($x = 0.20$–0.40) membranes exhibit a tendency to a reduced role of the surface exchange limitations with decreasing temperature—the difference between $J(O_2)$ values of the membranes with different thicknesses tends to become insignificant when temperature decreases (Figs. 7 and 9). In particular, the values of the oxygen permeability of $Sr_{0.97}Ti_{0.60}Fe_{0.40}O_{3-\delta}$ in the thickness range from 1 to 2 mm at 1073 K are similar within the experimental error limits (Fig. 9), indicating that the oxygen transport through STF40 membranes is predominantly limited by the bulk ionic conduction. This suggests a higher activation energy for the oxygen ionic conductivity in comparison with the activation energy for surface exchange. The greater values of the activation energy for ionic conduction in comparison with that of oxygen interphase exchange are typical for numerous perovskite-type oxides such as $La_{0.3}Sr_{0.7}CoO_{3-\delta}$[28] or $La_{0.6}Sr_{0.4}Fe_{0.8}CoO_{3-\delta}$.[29]

In contrast to $Sr_{0.97}Ti_{0.80}Fe_{0.20}O_{3-\delta}$ and $Sr_{0.97}Ti_{0.60}Fe_{0.40}O_{3-\delta}$, no tendency to a decreased role of the exchange limitations with reducing temperature was observed for the $Sr_{0.97}Ti_{0.70}Fe_{0.20}Mg_{0.10}O_{3-\delta}$ membranes (Fig. 8). More detailed studies are necessary in order to determine the reasons for such behavior, which is probably associated with a higher ionic conductivity and lower surface exchange rate of STF2M1 with respect to STF40 at temperatures below 1073 K.

4 Relationship between oxygen permeation and faradaic efficiency data

It has been seen that slow surface exchange kinetics may limit the oxygen permeation fluxes through $Sr_{0.97}T_{1-x-y}Fe_xMg_yO_{3-\delta}$ materials. As previously discussed,[15,18,30,31] the ion transference numbers obtained from oxygen permeation results tend to be underestimated if surface exchange affects the permeation flux. The phenomena involved in a permeation cell are similar to those happening in a faradaic efficiency measurement, and the possible effects of surface exchange limitations on faradaic efficiency results should also be analysed. Let us consider the following simplified model in order to compare the experimental data obtained by the different techniques.

Estimations of t_o values from oxygen permeation data can be obtained from the observed ambipolar conductivity (see eqn. (3)):

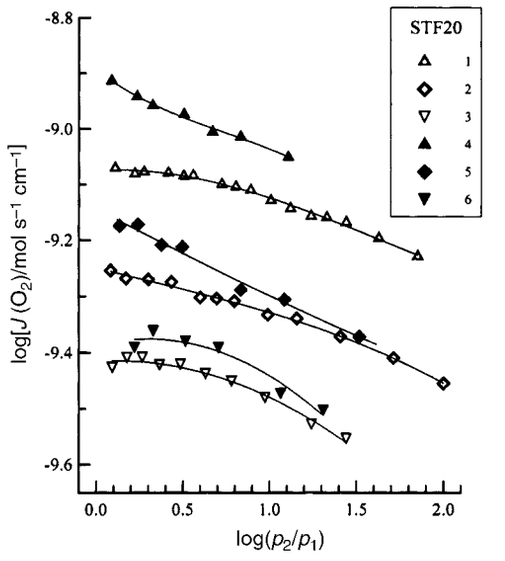

Fig. 7 Dependence of the specific oxygen permeability of the $Sr_{0.97}Ti_{0.80}Fe_{0.20}O_{3-\delta}$ membranes with $d = 0.90$ mm (curves 1–3) and 1.40 mm (4–6) on the oxygen pressure gradient: (1) and (4), 1173 K; (2) and (5), 1123 K; (3) and (6), 1073 K. Curves (4–6) correspond to the membrane with the porous $Sr_{0.97}Ti_{0.80}Fe_{0.20}O_{3-\delta}$ layer on the feed-side surface.

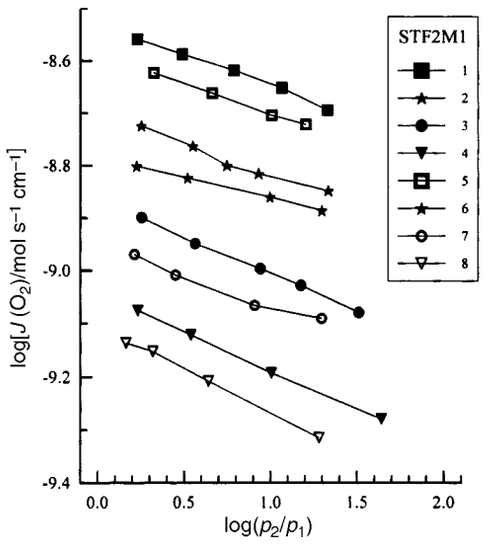

Fig. 8 Dependence of the oxygen permeability of the $Sr_{0.97}Ti_{0.70}Fe_{0.20}Mg_{0.10}O_{3-\delta}$ membranes with $d = 0.90$ mm (curves 1–4) and 0.60 mm (5–8) on the oxygen pressure gradient: (1) and (5), 1173 K; (2) and (6), 1123 K; (3) and (7), 1073 K; (4) and (8), 1023 K.

Table 3 Ionic transport numbers in air of $Sr_{0.97}Ti_{1-x-y}Fe_xMg_yO_{3-\delta}$ determined from the faradaic efficiency results

Composition	T/K	t_o^{obs}
$Sr_{0.97}Ti_{0.70}Fe_{0.20}Mg_{0.10}O_{3-\delta}$	1223	0.115
	1173	0.080
$Sr_{0.97}Ti_{0.60}Fe_{0.40}O_{3-\delta}$	1223	0.041
	1173	0.033
	1073	0.0090
	973	0.0050

$$\sigma_{amb}^{obs} = \frac{d}{S}\cdot\left(\frac{\partial I_{out}}{\partial E}\right)_{E\to 0} \quad (11)$$

$$t_o = \frac{1}{2} - \frac{1}{2}\sqrt{1-4\,\frac{\sigma_{amb}^{obs}}{\sigma}} \quad (12)$$

However, if surface exchange kinetics are slow, the estimation of the bulk ionic transport parameters from oxygen permeation results is associated with significant theoretical limitations.[21]

A schematic representation of the transport processes and equivalent circuits of a mixed-conducting membrane, placed under either an oxygen chemical potential gradient (oxygen permeation cell) or an electrical potential gradient (faradaic efficiency cell), are given in Fig. 10. For simplicity, the latter is considered when the oxygen pressure gradient is zero (eqn. (7) and (9)).

In a simplified case when all the transport parameters are independent of the oxygen chemical potential, the oxygen flux in the permeation cell (Fig. 10A), expressed in electrical units, can be written as

$$j\cdot 4F = [R_o + R_e + R_\eta]^{-1}\cdot\frac{E}{S} = \left[\frac{d}{\sigma_o} + \frac{d}{\sigma_e} + \frac{1}{K_{ex}}\right]^{-1}\cdot E = \frac{\sigma_o\sigma_e\cdot K_{ex}}{d\sigma_e K_{ex} + d\sigma_o K_{ex} + \sigma_o\sigma_e}\,E \quad (13)$$

where S is the membrane surface area, R_o and R_e (Ohm) are the partial ionic and electronic resistances, respectively, R_η (Ohm) is the sum of the polarization resistances at the membrane permeate and feed sides, K_{ex} is the coefficient of proportionality between the oxygen flux density through gas/oxide boundaries and the sum of oxygen chemical potential differences across these boundaries ($\Delta\mu$):

$$K_{ex} = [R_\eta\cdot S]^{-1} = \frac{j\cdot 16F^2}{\Delta\mu} \quad (14)$$

Therefore, the observed transference numbers which can be calculated by eqn. (12) in case of non-negligible surface exchange limitations relate to the true values of t_o as

$$t_o^{obs} = \frac{1}{2} - \frac{1}{2}\sqrt{\frac{1-4t_o(1-t_o)}{W}} \quad (15)$$

where

$$W = 1 + \frac{1}{(K_{ex}\cdot d/\sigma_e) + (K_{ex}\cdot d/\sigma_o)} \quad (16)$$

As a result, true values of the oxygen ion transference numbers can be obtained from the oxygen permeation data under conditions of either negligible surface exchange limitations or sufficiently thick samples, when $K_{ex}\times d \gg \sigma_o, \sigma_e$. In other cases, the transference numbers estimated from the permeation data are expected to be lower than the true values.

The equivalent circuit for faradaic efficiency measurements is similar but the electronic branch is parallel to the ionic one (Fig. 10B). The equations for total current (I_{in}) and for oxygen flux expressed in electrical units (I_{out}) can be represented as

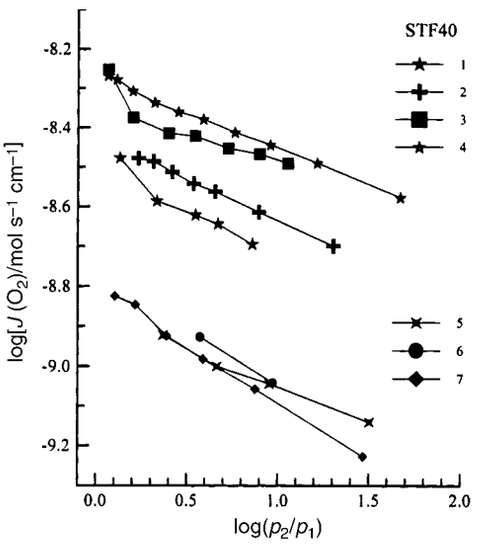

Fig. 9 Dependence of the oxygen permeability of the $Sr_{0.97}Ti_{0.60}Fe_{0.40}O_{3-\delta}$ membranes on the oxygen pressure gradient at 1173 K (1–4) and 1073 K (5–7): (1), d=1.28 mm; (2), d=2.00 mm; (3), d=1.00 mm, membrane with the Pt/PrO_x layer on the feed-side surface; (4), d=1.75 mm, membrane with the porous STF40 layer on the feed-side surface; (5), d=1.00 mm; (6), d=1.28 mm; (7), d=2.00 mm.

$$I_{in} = \left[\frac{1}{R_o + R_\eta} + \frac{1}{R_e}\right]\cdot U = \frac{d\sigma_e K_{ex} + d\sigma_o K_{ex} + \sigma_o\sigma_e}{d^2 K_{ex} + d\sigma_o}\cdot SU \quad (17)$$

$$I_{out} = \frac{U}{R_o + R_\eta} = \frac{\sigma_o K_{ex}}{dK_{ex} + \sigma_o}\cdot SU \quad (18)$$

where U is the voltage applied to the sample under tests, and R_η corresponds to the classical definition of the polarization resistance. Note that under steady state conditions the oxygen flux through the sample is equal to the oxygen flux pumped out of the cell ($I_{out}/4F$); the flux through the sample should be calculated considering only the right branch of the equivalent circuit shown in Fig. 10B. Substituting eqn. (17) and (18) into eqn. (9), one obtains

$$t_o^{obs} = t_o\cdot W^{-1} \quad (19)$$

where the parameter W is defined by eqn. (16).

Hence, the values of transference numbers determined from the faradaic efficiency data can be also underestimated due to slow oxygen surface exchange (high polarization resistance of the electrodes). Analogously to the oxygen permeation results, this effect can be negligible only if the partial ionic resistance is much higher than the polarization resistance, or if the thickness of the sample is sufficiently large, when

$$W \approx 1 \quad (20)$$

One should separately note that, even under identical conditions, the oxygen exchange currents in the oxygen permeation and faradaic efficiency cells may be different, due to both catalytically-active Pt electrodes in the case of faradaic efficiency and to different oxygen discharge mechanisms. Therefore, the quantitative effect of the surface-exchange limitations on the measured transference numbers may be different in these two cases. This is illustrated by Fig. 11 showing various mechanisms of oxygen discharge. For the case of oxygen permeation, oxygen sorption and discharge should occur either on all the surface or at electrocatalytically-active centers at the surface. In the latter case, an additional step of surface diffusion may take place. For faradaic efficiency, however, the discharge process should certainly include the stage of charge carrier transport to the current collector, which may occur in various ways. Fig. 11B shows, as examples of

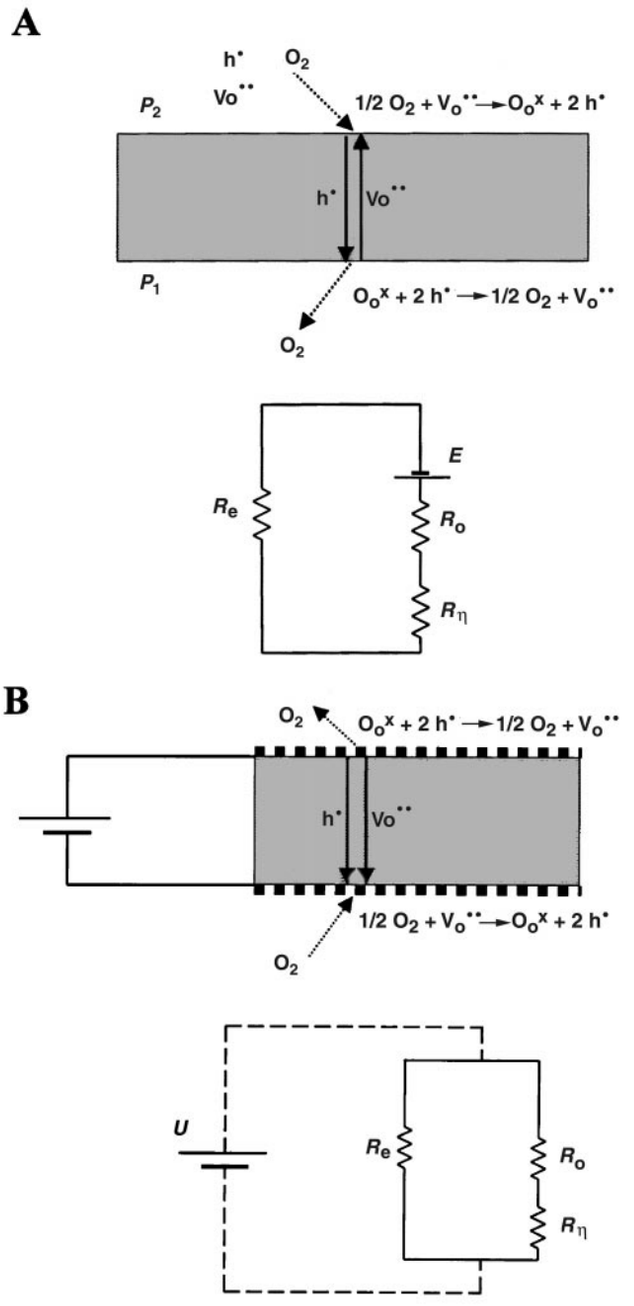

Fig. 10 Schematic representation and equivalent circuit of a mixed-conducting membrane placed in oxygen permeation cell (A) and faradaic efficiency cell (B). The driving force is the e.m.f. (E) in the case of oxygen permeation and the applied voltage (U) in the case of faradaic efficiency.

such ways, a transfer of oxygen ions along the membrane surface (left), surface diffusion of adsorbed oxygen species (center), and transport of electron holes to the current collector after oxygen molecule discharged at the surface (right). There may also be other possible discharge mechanisms. However, the discharge in faradaic efficiency cells always includes an additional stage in comparison with the permeation process. This may lead to higher R_η values and, therefore, lower observed ion transference numbers in the case of faradaic efficiency measurements with respect to oxygen permeation data. At the same time, the presence of catalytically active platinum on the membrane surface in the course of faradaic efficiency tests could result in increasing exchange currents.

Another important factor affecting the transference numbers, determined by the different techniques, refers to the fact that both p-type electronic and ionic conductivity of

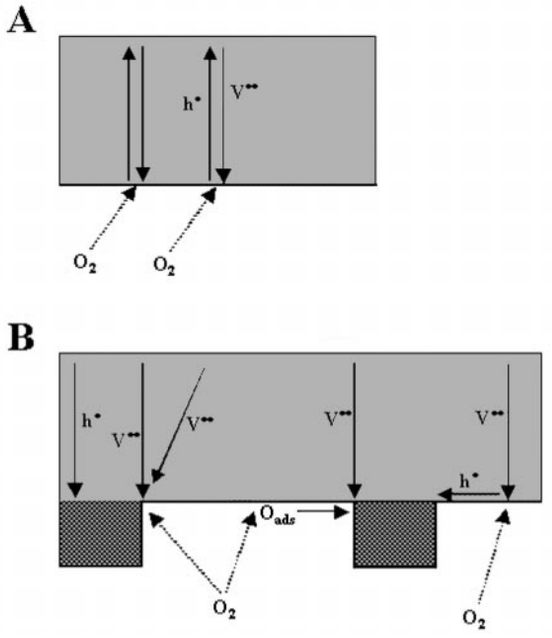

Fig. 11 Schematic representation of the differences in oxygen discharge mechanisms for oxygen permeation (A) and faradaic efficiency (B) electrochemical cells.

$Sr_{0.97}Ti_{1-x-y}Fe_xMg_yO_{3-\delta}$ are functions of oxygen partial pressure. The p-type electronic conduction decreases with decreasing oxygen pressure,[3] whilst the ionic transport behaviour is expected to be opposite due to increasing oxygen vacancy concentration when $p(O_2)$ decreases.[21] As a result, the oxygen transference number should increase with increasing oxygen content in the gas phase. Experimental observations confirm such a statement (Fig. 12). Therefore, an estimation of the transference numbers from the oxygen permeation data is possible only in a narrow oxygen-pressure range where the dependence of the partial conductivities on the oxygen chemical potential can be neglected, or if the defect chemistry is known, including possible interaction between ionic and electronic defects.

5 Faradaic efficiency results

Fig. 13 presents the ion transference numbers of $Sr_{0.97}Ti_{0.70}Fe_{0.20}Mg_{0.10}O_{3-\delta}$ and $Sr_{0.97}Ti_{0.60}Fe_{0.40}O_{3-\delta}$ ceramics in air, estimated from the data on faradaic efficiency and oxygen permeation using eqn. (9) and (12), respectively. The observed

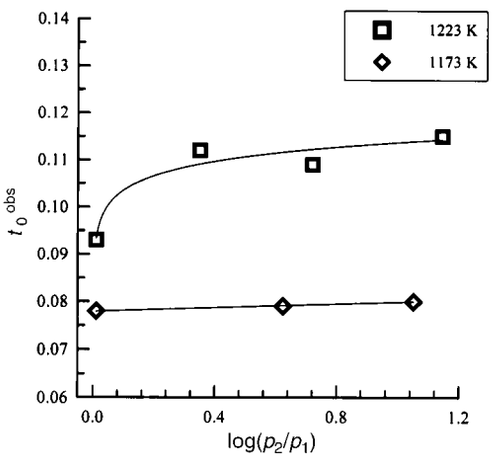

Fig. 12 Oxygen ion transference numbers of $Sr_{0.97}Ti_{0.70}Fe_{0.20}Mg_{0.10}O_{3-\delta}$, determined from the faradaic efficiency results, as functions of temperature and oxygen partial pressure gradient. The membrane thickness is 0.90 mm. The solid lines are for visual guidance only.

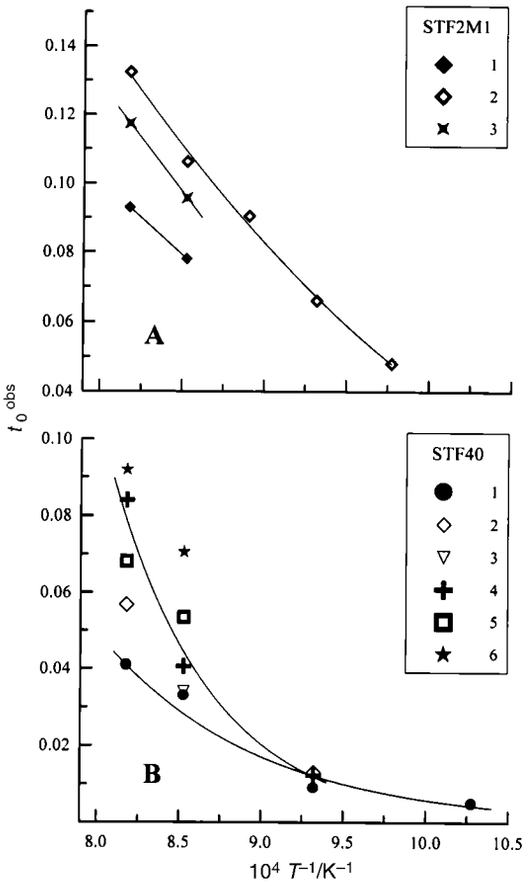

Fig. 13 Temperature dependence of the observed oxygen ion transference numbers in air: A—STF2M1 membranes: (1), FE, $d=0.90$ mm; (2), OP, $d=0.90$ mm; (3), OP, $d=0.60$ mm. B—STF40 membranes: (1), FE, $d=1.00$ mm; (2), OP, $d=1.00$ mm; (3), OP, $d=1.28$ mm; (4), OP, $d=2.00$ mm; (5), OP, $d=1.00$ mm, Pt/PrO_x layer; (6), OP, $d=1.75$ mm, porous STF40 layer. The solid lines are for visual guidance only.

t_o values increase with increasing membrane thickness, as expected from the decrease of the relative role of surface exchange. Surface modification of membranes also leads to higher estimations of the transference numbers. In general, the values of t_o obtained from the faradaic efficiency data are lower than estimations from oxygen permeability, suggesting the existence of different discharge mechanisms in these two cases. However, an exception occurs with the $Sr_{0.97}Ti_{0.60}Fe_{0.40}O_{3-\delta}$ material at $T\leqslant 1073$ K. Similar values of oxygen permeability for membranes with various thicknesses (Fig. 9) suggest a negligible effect of surface exchange on the permeation under such conditions. In fact, the ion transference number obtained from faradaic efficiency data is close to the estimations from oxygen permeation data (Fig. 13). This substantiates the above conclusions that the role of the exchange processes decreases with decreasing temperature and, in particular, that oxygen permeation through $Sr_{0.97}Ti_{0.60}Fe_{0.40}O_{3-\delta}$ at 1073 K is limited by the bulk ionic conductivity.

The observed values of the ion transference numbers determined from faradaic efficiency data in air are listed in Table 3. With the exception of $Sr_{0.97}Ti_{0.60}Fe_{0.40}O_{3-\delta}$ at temperatures below 1100 K, all the faradaic efficiency results on the ion trasference number values are affected by surface limitations and should be seen as crude approximations. At 1223 K, the true t_o value for $Sr_{0.97}Ti_{0.60}Fe_{0.40}O_{3-\delta}$ was thus estimated to be between 0.04 and 0.09, whereas the ion transference number of $Sr_{0.97}Ti_{0.70}Fe_{0.20}Mg_{0.10}O_{3-\delta}$ is as high as 0.12–0.14 due to the lower electronic conductivity of this solid solution.

The temperature dependence of the observed oxygen ionic conductivity of $Sr_{0.97}Ti_{0.60}Fe_{0.40}O_{3-\delta}$ and $Sr_{0.97}Ti_{0.70}Fe_{0.20}Mg_{0.10}O_{3-\delta}$ ceramics in air, calculated as

$$\sigma_o^{obs} = t_o^{obs}\cdot\sigma \qquad (21)$$

is given in Fig. 14. For comparison, the conductivity of the widely-used solid electrolyte $Zr_{0.92}Y_{0.08}O_{1.96}$[32] is also presented. The data suggest that titanium substitution with magnesium provides the same effect on ionic conduction as the incorporation of large amounts of iron into the B sublattice. Since the oxidation state of Mg^{2+} is stable, this feature may be useful from the viewpoint of stability of the perovskites in reducing environments, where reduction of iron cations lead to thermodynamic and dimensional instability of the perovskites.

When comparing the ionic conductivity of $Sr_{0.97}Ti_{1-x-y}Fe_xMg_yO_{3-\delta}$ and YSZ, one should note that at temperatures above 1170 K ionic conduction in $Sr_{0.97}Ti_{0.60}Fe_{0.40}O_{3-\delta}$ tends to be close to that in yttria-stabilized zirconia (Figs. 13 and 14), in agreement with previous results.[15] At lower temperatures, however, oxygen transport is still low for applications in electrochemical cells, requiring further improvements of the ionic conductivity of $Sr_{0.97}Ti_{1-x-y}Fe_xMg_yO_{3-\delta}$ solid solutions.

Conclusions

Ceramic membranes of perovskite-type $Sr_{0.97}Ti_{1-x-y}Fe_xMg_yO_{3-\delta}$ ($x=0.20$–0.40; $y=0$–0.10) solid solutions were prepared by the standard ceramic synthesis route with densities higher than 95% of the theoretical value. Both p-type electronic and ionic conductivies of the strontium titanate-based solid solutions were found to increase with increasing concentration of either iron or magnesium. TGA/DTA in different atmospheres demonstrated the stability of the materials with respect to the reaction with carbon dioxide at temperatures above 770 K. However, exposure of the oxides to a CO_2-containing atmosphere at lower temperatures may result in surface decomposition of the perovskite, associated with the formation of strontium carbonate.

A non-negligible polarization resistance of the cells for faradaic efficiency studies was shown to affect the measured ion transference numbers, decreasing them with respect to their

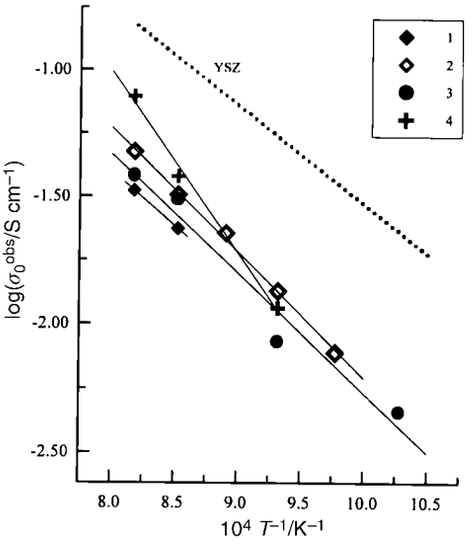

Fig. 14 Temperature dependence of the observed oxygen ionic conductivity of $Sr_{0.97}Ti_{0.70}Fe_{0.20}Mg_{0.10}O_{3-\delta}$ (1, 2) and $Sr_{0.97}Ti_{0.60}Fe_{0.40}O_{3-\delta}$ (3, 4) in air, calculated from the results of faradaic efficiency (1, 3) and oxygen permeability (2, 4) tests. The membrane thickness is: (1) and (2), 0.90 mm; (3), 1.00 mm; (4), 2.00 mm. Solid lines correspond to the fitting results using an Arrhenius model. The data on YSZ from ref. 29 are shown for comparison.

true values. A similar effect is typical for the transport parameters (ionic or ambipolar conductivities, ion transference numbers) calculated from the oxygen permeability results when surface exchange limitations take place. For both faradaic efficiency and oxygen permeation studies, the effect of the surface exchange on the measured bulk transport properties can be detected by comparing the data on samples with different thicknesses; this influence may be subsequently avoided by choosing an appropriate thickness. Alternatively, a comparison of the results of different measurement techniques is necessary in order to verify the obtained bulk transference parameters.

The results of oxygen permeation and faradaic efficiency studies of $Sr_{0.97}Ti_{1-x-y}Fe_xMg_yO_{3-\delta}$ ceramics suggest that permeation fluxes are limited by both bulk ionic conductivity and surface exchange rates. For $Sr_{0.97}(Ti,Fe)O_{3-\delta}$ solid solutions, the role of the surface exchange as the permeation-determining factor decreases with reducing temperature. In particular, oxygen permeation fluxes through $Sr_{0.97}Ti_{0.60}Fe_{0.40}O_{3-\delta}$ at temperatures below 1100 K are limited predominantly by the bulk ionic conduction. In contrast, the limiting effect of the interphase exchange on oxygen transport through $Sr_{0.97}Ti_{0.70}Fe_{0.20}Mg_{0.10}O_{3-\delta}$ membranes is observed to be significant within the studied temperature range, suggesting that doping with magnesium leads to a higher ionic conductivity and lower surface exchange rates in comparison with $Sr_{0.97}Ti_{0.60}Fe_{0.40}O_{3-\delta}$ perovskite which exhibits similar permeation fluxes.

Acknowledgements

This research was partially supported by the FCT, Portugal (Praxis program and Project P/CTM/14170/1998), the Belarus Foundation for Basic Research, and the Belarus Ministry of Education and Science.

References

1 H. Iwahara, *Solid State Ionics*, 1992, **52**, 99.
2 S. Sekido, H. Tachibara, Y. Yamamura and T. Kambara, *Solid State Ionics*, 1990, **37**, 253.
3 L. S. M. Traqueia, J. R. Jurado and J. R. Frade, in *Proc. Int. Conf. Electroceramics V, Aveiro, Portugal,*, ed. J. L. Baptista, J. A. Labrincha and P. M. Vilarinho, Fundaçao Joao Jacinto de Magalhaes, Aviero, 1996, vol. 2, p. 151.
4 H. Itoh, H. Asano, K. Fukuroi, M. Nagata and H. Iwahara, *J. Am. Ceram. Soc.*, 1997, **80**, 1359.
5 I. Denk, F. Noll and J. Maier, *J. Am. Ceram. Soc.*, 1997, **80**, 279.
6 V. V. Kharton, S.-B. Li, A. V. Kovalevsky and E. N. Naumovich, *Solid State Ionics*, 1997, **96**, 141.
7 V. P. Gorelov and V. B. Balakireva, *Elektrokhimiya*, 1997, **33**, 1450 [in Russian].
8 V. V. Kharton, S.-B. Li, A. V. Kovalevsky, A. P. Viskup, E. N. Naumovich and A. A. Tonoyan, *Mater. Chem. Phys.*, 1998, **53**, 6.
9 J. R. Jurado, F. M. Figueiredo, B. Charbage and J. R. Frade, *Solid State Ionics*, 1999, **118**, 89.
10 T. Kawada, T. Watanabe, A. Kaimai, K. Kamamura, Y. Nigara and J. Mizusaki, *Solid State Ionics*, 1998, **108**, 391.
11 T. J. Mazanec, T. L. Cable, J. G. Frye and W. R. Kliewer, *US Patent* 5 744 015, 1998.
12 S. Xie, W. Liu, K. Wu, P. H. Yang, G. Y. Meng and C. S. Chen, *Solid State Ionics*, 1999, **118**, 23.
13 L. A. Dunyushkina, A. K. Demin and B. V. Zhuravlev, *Solid State Ionics*, 1999, **116**, 85.
14 S. R. Song and H.-I. Yoo, *Solid State Ionics*, 1999, **120**, 141.
15 J. R. Jurado, F. M. Figueiredo and J. R. Frade, *Solid State Ionics*, 1999, **122**, 197.
16 M. F. Carolan, P. N. Dyer, J. M. LaBar and R. M. Thorogood, *US Patent* 5 261 932, 1993.
17 M. F. Carolan, P. N. Dyer, S. A. Motika and P. B. Alba, *US Patent* 5 712 220, 1998.
18 V. V. Kharton, A. V. Kovalevsky, A. P. Viskup, F. M. Figueiredo, J. R. Frade, A. A. Yaremchenko and E. N. Naumovich, *Solid State Ionics*, 2000, **128**, 117.
19 V. V. Kharton, E. N. Naumovich, A. A. Vecher and A. V. Nikolaev, *J. Solid State Chem.*, 1995, **120**, 128.
20 A. A. Yaremchenko, V. V. Kharton, A. P. Viskup, E. N. Naumovich, N. M. Lapchuk and V. N. Tikhonovich, *J. Solid State Chem.*, 1999, **142**, 225.
21 V. V. Kharton, V. N. Tikhonovich, S.-B. Li, E. N. Naumovich, A. V. Kovalevsky, A. P. Viskup, I. A. Bashmakov and A. A. Yaremchenko, *J. Electrochem. Soc.*, 1998, **145**, 1363.
22 V. V. Kharton, A. P. Viskup, E. N. Naumovich and F. M. B. Marques, *J. Mater. Chem.*, 1999, **9**, 2623.
23 V. V. Kharton, A. P. Viskup, E. N. Naumovich, A. A. Tonoyan and O. P. Reut, *Mater. Res. Bull.*, 1998, **33**, 1087.
24 H.-H. Moebius, in *Extended Abstracts 37th Meet. ISE*, ISE, Vilnius, Lithuania, 1986, **vol. 1**, p. 136.
25 V. V. Kharton, E. N. Naumovich, A. V. Kovalevsky, A. A. Yaremchenko, A. P. Viskup and P. F. Kerko, *J. Membr. Sci.*, 1999, **163**, 307.
26 A. V. Kovalevsky, V. V. Kharton and E. N. Naumovich, *Mater. Lett.*, 1999, **38**, 300.
27 *Handbook of Infrared and Raman Spectra of Inorganic Compounds and Organic Salts. Vol. 4: IR Spectra of Inorganic Compounds*, ed. R. A. Nyquist and R. O. Kagel, Academic Press, San Diego–London–Boston–NY–Sydney–Tokyo–Toronto, 1997.
28 R. H. E. van Doorn, I. C. Fullarton, R. A. de Souza, J. A. Kilner, H. J. M. Bouwmeester and A. J. Burggraaf, *Solid State Ionics*, 1997, **96**, 1.
29 S. J. Benson, R. J. Chater and J. A. Kilner, in *Ionic and Mixed Conducting Ceramics III*, ed. T. A. Ramanarayanan, The Electrochemical Society, Pennington, NJ, 1998, Proceedings Volume 97–24, p. 596.
30 R. M. Thorogood, R. Srinivasan, T. F. Yu and M. P. Drake, *US Patent* 5 240 480, 1993.
31 M. Liu, in *Ionic and Mixed Conducting Oxides*, ed. T. A. Ramanarayanan, W. L. Worrell and H. L. Tuller, The Electrochemical Society, Pennington, NJ, 1994, Proceedings Volume 94–12, p. 191.
32 S. P. Badwal, *Solid State Ionics*, 1992, **52**, 23.